IEEE Transactions on Antennas and Propagation, to be published

Systematic Design of Multimode Antennas for MIMO Applications by Leveraging Symmetry

Authors:
Nikolai Peitzmeier
Tim Hahn
Dirk Manteuffel

Suggested Citation:
N. Peitzmeier, T. Hahn and D. Manteuffel, "Systematic Design of Multimode Antennas for MIMO Applications by Leveraging Symmetry", *IEEE Transactions on Antennas and Propagation, to be published,* 2021

Systematic Design of Multimode Antennas for MIMO Applications by Leveraging Symmetry

Nikolai Peitzmeier, *Member, IEEE,* Tim Hahn, and Dirk Manteuffel, *Member, IEEE*

***Abstract*—A systematic procedure for constructing orthogonal antenna ports on arbitrary symmetric multimode antennas is proposed. The procedure is based on the projection operator method from group theory. With this method, optimal orthogonal port configurations are generated analytically. Electromagnetic simulations, modal analyses, or optimization techniques are not required. The optimal port configurations are solely governed by the symmetry of an antenna and can thus be considered as a priori knowledge. Accordingly, this knowledge is available right from the beginning of the design process and can be purposefully used to compare different suitable antenna geometries with respect to the practical implementation effort. The procedure is illustrated by means of an application example resulting in a complete prototype of a six-port multimode antenna.**

***Index Terms*—Characteristic modes, multimode antenna, symmetry, group theory, antenna theory, antenna diversity.**

I. Introduction

THE application of multimode antennas in multiple-input multiple-output (MIMO) systems is a promising, space-efficient alternative to using multiantenna architectures. In conventional antenna arrays, the elements need to be located spatially apart in order to provide spatial diversity [1], [2]. In contrast, multimode antennas consist of a single physical antenna element with several independent antenna ports offering a combination of pattern and polarization diversity [3]. Ideally, each port of a multimode antenna drives a specific antenna mode with distinct radiation pattern and polarization. This way, uncorrelated antenna ports are created, which is most beneficial for MIMO performance [4], [5].

Over the past decade, the theory of characteristic modes [6]–[8] has been employed extensively in order to design multimode antennas in an intuitive way. This design approach is based on the fact that the characteristic modes of an antenna possess advantageous orthogonality properties [7]. The ports of a multimode antenna are thus intended to excite mutually exclusive sets of characteristic modes [9]. This way, perfectly uncorrelated (orthogonal) antenna ports can be realized.

As proposed in early pioneering work [10]–[14], suitable antenna ports are defined by inspecting the surface current densities of the characteristic modes. In order to reproduce the desired modal behavior, feed points are distributed on the antenna element. A single antenna port consists of several such feed points which are driven simultaneously by means of a feed network. More recent designs basically rely on the same concept, yielding compact multimode antennas with up to four perfectly uncorrelated ports [15]–[17].[1]

Unfortunately, this intuitive design approach has its limitations. In order to excite different characteristic modes separately, their respective surface current densities need to be uncorrelated [9]. However, this is in general not guaranteed by the theory of characteristic modes.[2] As a consequence, an antenna port that is supposed to excite a certain characteristic mode will generally also excite all those modes whose surface current densities are correlated. This limits the degrees of freedom for realizing orthogonal antenna ports (cf. [18], [19]).

The correlation of the characteristic surface current densities is related to the symmetry of an antenna [19]. Only symmetric antenna geometries provide mutually orthogonal sets of characteristic surface current densities, and only these sets of modes can be excited separately by appropriately designed antenna ports [9]. However, the number of these sets is dictated by the symmetry of an antenna and is thus limited, regardless of the number of modes taken into account. Consequently, there is an upper bound for orthogonal antenna ports which is solely governed by the symmetry of an antenna [9].

The exploitation of symmetries has recently sparked considerable interest in the context of characteristic modes [9], [20]–[24]. Interestingly, all the above-mentioned pioneering multimode antenna designs [10]–[17] can be explained within the framework of the symmetry analysis presented in [9]. In fact, leveraging symmetries can be considered the natural extension of the intuitive design approach based on characteristic modes. A first step in this regard is proposed in [22], [23], where point group theory is utilized in order to enable uncorrelated MIMO channels. These works demonstrate the principal benefits of exploiting symmetries for antenna design. However, the derived idealized feeding scheme is only available within a method of moments (MoM) framework and practical design consequences are not discussed.

Therefore, this work aims at combining a thorough theoretical analysis with direct implications for a practical antenna design. Exploiting the connection between the characteristic modes of an antenna and its symmetry, a systematic and automated design procedure for arbitrary symmetric multimode antennas is proposed. It is demonstrated that the optimal port configurations are governed by the symmetry of a given antenna geometry alone. Thus, a characteristic mode analysis

This work was supported by Deutsche Forschungsgemeinschaft (DFG) within the priority program SPP 1655 under grant MA 4981/4-2.

The authors are with the Institute of Microwave and Wireless Systems, Leibniz University Hannover, Hannover 30167, Germany, (e-mail: peitzmeier@imw.uni-hannover.de; manteuffel@imw.uni-hannover.de).

[1]The terms *perfectly uncorrelated* and *orthogonal* are employed in order to emphasize that a design concept ideally yields antenna ports with zero correlation, as e.g. presented in this work. This is in contrast to design strategies which accept a certain level of correlation from the start, e.g. [18].

[2]The characteristic surface current densities are orthogonal with respect to the impedance operator, but are not necessarily directly orthogonal to each other. This is only true for the characteristic far fields [7].

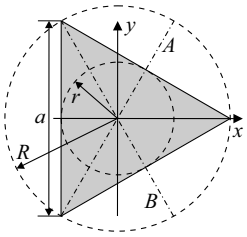

(a)

Symmetry Operation	T
Identity	E
Rotation by 120° about z-axis	C_{3z}
Rotation by 240° about z-axis	C_{3z}^2
Rotation by 180° about x-axis	C_{2x}
Rotation by 180° about axis A	C_{2A}
Rotation by 180° about axis B	C_{2B}

(b)

Fig. 1. Equilateral triangular plate. (a) Geometry. (b) Symmetry operations.

is not even required. Instead, a priori knowledge about the optimal port configurations is gained completely analytically.

To this end, the construction of orthogonal antenna ports is explained in section II. An application example is discussed in section III, where a desired number of orthogonal antenna ports are constructed. The resulting fabricated prototype is presented in section IV and its performance is evaluated.

II. Port Construction Procedure

The proposed port construction procedure is based on the fundamental connection between the characteristic modes of an antenna and its symmetry [25]. This connection is briefly recapped in an illustrative way. Then, the so-called projection operators are introduced and exploited in order to construct orthogonal antenna ports analytically.

A. Fundamentals

In order to realize orthogonal antenna ports, mutually orthogonal sets of characteristic surface current densities are required [9]. As an example, Table I lists a selection of twelve characteristic surface current densities on an equilateral triangular plate (Fig. 1(a)). The correlation of these current densities is shown in Fig. 2. Four mutually orthogonal sets of characteristic surface current densities are identified. The modes are sorted accordingly. It is noticed that the characteristic surface current densities belonging to the same set possess the same symmetry properties [19]. In order to quantify this observation, the theory of symmetry has to be applied.

The coordinate transformations which leave an antenna invariant (symmetry operations) form the so-called symmetry group of the antenna [26]. For example, the symmetry group of the equilateral triangular plate contains the six operations listed in Fig. 1(b) [27]. The number of symmetry operations is called the group order g (here: $g = 6$).

The principal question is how the characteristic surface current densities are affected by such symmetry operations. Mathematically, the effect of an arbitrary symmetry operation T on some vector-valued function $\mathbf{f}(\mathbf{r}) : \mathbb{R}^3 \to \mathbb{C}^3$ is described by the transformation operator $P(T)$ [28]. The transformed function $\mathbf{f}'(\mathbf{r})$ is written as

$$\mathbf{f}'(\mathbf{r}) = P(T)\mathbf{f}(\mathbf{r}) = \mathbf{R}(T)\mathbf{f}\big(\mathbf{R}^{\mathrm{T}}(T)\mathbf{r}\big), \tag{1}$$

with $\mathbf{r} = (x, y, z)^{\mathrm{T}}$. $\mathbf{R}(T)$ is the rotation matrix representing the symmetry operation T, which can be readily computed for any rotation according to [28] (see appendix A).

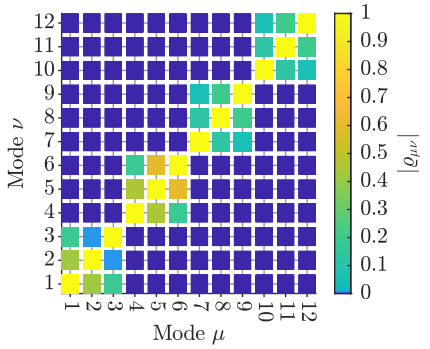

Fig. 2. Correlation coefficients $|\varrho_{\mu\nu}|$ of the characteristic surface current densities from Table I. Dark blue is equal to zero.

TABLE I
Selected Characteristic Surface Current Densities of Equilateral Triangular Plate with $R = 0.6$ Wavelengths and Assignment to Irreducible Representations.

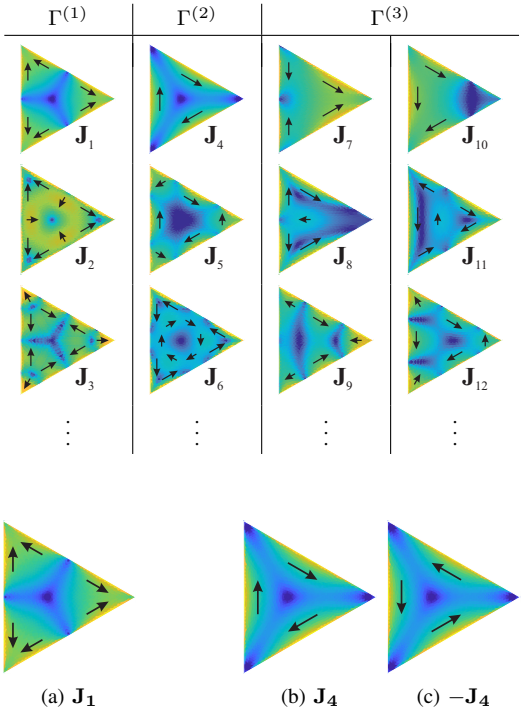

(a) $\mathbf{J_1}$ (b) $\mathbf{J_4}$ (c) $-\mathbf{J_4}$

Fig. 3. Transformation of characteristic surface current densities. (a) $\mathbf{J}_1$ is invariant under all six symmetry operations: $P(T)\mathbf{J}_1 = \mathbf{J}_1 \; \forall \; T \in \mathcal{G}$. (b) $\mathbf{J}_4$ is invariant under the identity and the rotations about the z-axis: $P(T)\mathbf{J}_4 = +\mathbf{J}_4$ for $T \in \{E, C_{3z}, C_{3z}^2\}$. (c) $\mathbf{J}_4$ is inverted by the rotations about the other axes: $P(T)\mathbf{J}_4 = -\mathbf{J}_4$ for $T \in \{C_{2x}, C_{2A}, C_{2B}\}$.

The transformation operators are now applied to the characteristic surface current densities, as exemplarily illustrated in Fig. 3. This way, it is found that all characteristic surface current densities of the equilateral triangular plate transform in one of four different ways (cf. Table I), namely according to the so-called irreducible representations of the symmetry group. The characteristic surface current densities are thus said to act as basis functions of the irreducible representations [25].

An irreducible representation assigns a representation matrix $\mathbf{\Gamma}^{(p)}(T)$ to each symmetry operation T of the group [28]. The elements $\Gamma_{mn}^{(p)}(T)$ of these matrices (row index m, column

TABLE II
REPRESENTATION MATRICES OF THE SYMMETRY GROUP OF THE EQUILATERAL TRIANGULAR PLATE.

	E	C_{3z}	C_{3z}^2	C_{2x}	C_{2A}	C_{2B}
$\mathbf{\Gamma}^{(1)}(T)$	1	1	1	1	1	1
$\mathbf{\Gamma}^{(2)}(T)$	1	1	1	-1	-1	-1
$\mathbf{\Gamma}^{(3)}(T)$	$\begin{pmatrix} 1 & 0 \\ 0 & 1 \end{pmatrix}$	$\begin{pmatrix} -1/2 & \sqrt{3}/2 \\ -\sqrt{3}/2 & -1/2 \end{pmatrix}$	$\begin{pmatrix} -1/2 & -\sqrt{3}/2 \\ \sqrt{3}/2 & -1/2 \end{pmatrix}$	$\begin{pmatrix} 1 & 0 \\ 0 & -1 \end{pmatrix}$	$\begin{pmatrix} -1/2 & \sqrt{3}/2 \\ \sqrt{3}/2 & 1/2 \end{pmatrix}$	$\begin{pmatrix} -1/2 & -\sqrt{3}/2 \\ -\sqrt{3}/2 & 1/2 \end{pmatrix}$

index n) describe the transformation of the characteristic surface current densities. A finite symmetry group possesses a finite number of irreducible representations. The p-th irreducible representation is denoted by the symbol $\Gamma^{(p)}$. It is said to be d_p-dimensional if the corresponding characteristic surface current densities are d_p-fold degenerate. The respective representation matrices $\mathbf{\Gamma}^{(p)}(T)$ are of dimension $d_p \times d_p$. For example, the symmetry group of the equilateral triangular plate has three irreducible representations $\Gamma^{(1)}$, $\Gamma^{(2)}$, and $\Gamma^{(3)}$ [27]. The first two ones are one-dimensional ($d_{1;2} = 1$), whereas the third one is two-dimensional ($d_3 = 2$). The corresponding representation matrices are listed in Table II.

Obviously, the irreducible representations arise naturally in conjunction with characteristic modes. Each characteristic surface current density can be assigned to exactly one irreducible representation [9] (e.g. see Table I). This assignment yields mutually orthogonal sets, as evidenced by Fig. 2. These sets of modes can be excited separately by antenna ports that, too, act as basis functions of the irreducible representations [9]. The equilateral triangular plate, for example, offers a maximum of four orthogonal antenna ports [9].

B. Projection Operators

The optimal port configurations have to act as basis functions of the irreducible representations. The projection operator method is an established technique from group theory whose purpose is to derive basis functions of irreducible representations [28], [29]. Therefore, it is ideally suited for the construction of orthogonal antenna ports.

The projection operator $\mathcal{P}_{mn}^{(p)}$ of the d_p-dimensional p-th irreducible representation $\Gamma^{(p)}$ of a finite symmetry group $\mathcal{G}$ of order g is defined as [28]

$$\mathcal{P}_{mn}^{(p)} = \frac{d_p}{g} \sum_{T \in \mathcal{G}} \Gamma_{mn}^{(p)*}(T) P(T), \quad m, n = 1, 2, \ldots, d_p. \quad (2)$$

A projection operator is a weighted sum of the transformation operators $P(T)$ over all symmetry operations T of the symmetry group $\mathcal{G}$. The weighting coefficients are the complex conjugate elements $\Gamma_{mn}^{(p)*}(T)$ of the representation matrices $\mathbf{\Gamma}^{(p)}(T)$ (e.g. Table II).

The application of the projection operator $\mathcal{P}_{mn}^{(p)}$ to an arbitrary function $\mathbf{f}(\mathbf{r})$ yields [28]

$$\mathcal{P}_{mn}^{(p)} \mathbf{f}(\mathbf{r}) = \gamma_n^{(p)} \mathbf{\psi}_m^{(p)}(\mathbf{r}), \quad (3)$$

where $\gamma_n^{(p)}$ is a weighting coefficient and $\mathbf{\psi}_m^{(p)}(\mathbf{r})$ is called the basis function belonging to the m-th row of the p-th irreducible representation. The application of the projection operator $\mathcal{P}_{mn}^{(p)}$ to an arbitrary function projects out of it the basis function which belongs to the m-th row of the p-th irreducible representation. This property is now made use of.

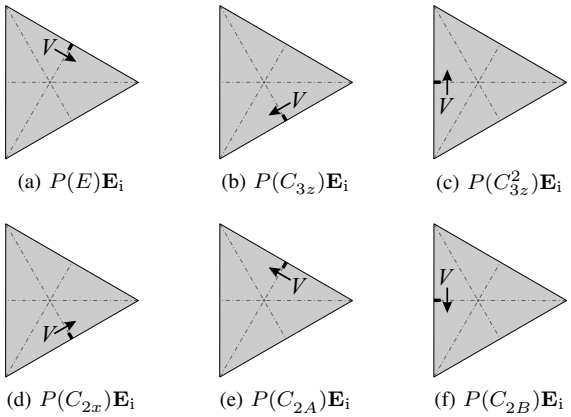

(a) $P(E)\mathbf{E}_\mathrm{i}$ (b) $P(C_{3z})\mathbf{E}_\mathrm{i}$ (c) $P(C_{3z}^2)\mathbf{E}_\mathrm{i}$

(d) $P(C_{2x})\mathbf{E}_\mathrm{i}$ (e) $P(C_{2A})\mathbf{E}_\mathrm{i}$ (f) $P(C_{2B})\mathbf{E}_\mathrm{i}$

Fig. 4. Transformation of the initial port configuration consisting of one delta-gap voltage source on the axis A due to the symmetry operations of the equilateral triangular plate. Delta-gap voltage sources denoted by black lines and arrows. (a) Original delta-gap voltage source (identity transformation). (b)–(f) Transformed delta-gap voltage sources. Computation in appendix A.

C. Construction of Orthogonal Antenna Ports

The port construction procedure is best illustrated by means of an example. The equilateral triangular plate offers four orthogonal antenna ports. The optimal port configurations are now derived by means of the projection operators.

An antenna port is represented by an impressed electric field strength. In order to enable an analytical treatment of the antenna ports, the feed points on the antenna are modeled as delta-gap voltage sources [30]. These can be readily replaced by excitation slots [31] at a later design stage (see section IV).

First of all, an initial port configuration has to be chosen from which the orthogonal antenna ports are constructed according to (3). It will become apparent throughout this subsection that a good choice is to place a single delta-gap voltage source on a symmetry axis (here: axis A), as illustrated in Fig. 4(a) and Fig. 5(a). The corresponding impressed electric field strength $\mathbf{E}_\mathrm{i}(\mathbf{r})$ is expressed as follows:

$$\mathbf{E}_\mathrm{i}(x, y) = V \delta\big(x - \frac{1}{2} r, y - \frac{\sqrt{3}}{2} r\big) \begin{pmatrix} \sqrt{3}/2 \\ -1/2 \end{pmatrix}, \quad (4)$$

where $\delta(\mathbf{r})$ is the Dirac delta function, V is an arbitrary source voltage, and r is the incircle radius according to Fig. 1.

For the computation of the projection operators, the transformation operators $P(T)$ are required. They are readily computed according to (1). The transformation of the initial port

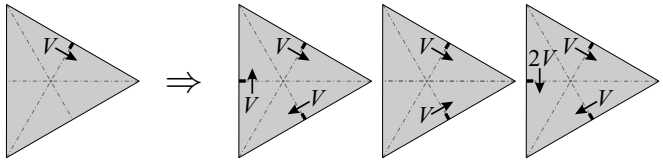

Fig. 5. Construction of orthogonal ports, part I. (a) Initial port configuration. (b) Port 2 belonging to $\Gamma^{(2)}$ constructed with operator $\mathcal{P}_{11}^{(2)}$. (c) Port 3 belonging to the first row of $\Gamma^{(3)}$ constructed with operator $\mathcal{P}_{11}^{(3)}$ or $\mathcal{P}_{12}^{(3)}$. (d) Port 4 belonging to the second row of $\Gamma^{(3)}$ constructed with operator $\mathcal{P}_{21}^{(3)}$ or $\mathcal{P}_{22}^{(3)}$. Delta-gap voltage sources denoted by black lines and arrows.

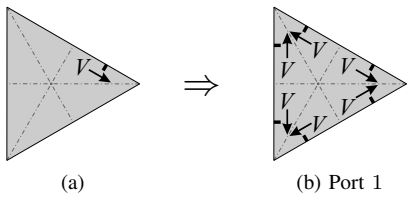

Fig. 6. Construction of orthogonal ports, part II. (a) Alternative initial port configuration. (b) Port 1 belonging to $\Gamma^{(1)}$ constructed with operator $\mathcal{P}_{11}^{(1)}$. Delta-gap voltage sources denoted by black lines and arrows.

configuration (4) under the symmetry operations of the equilateral triangular plate is illustrated in Fig. 4. The application of a projection operator $\mathcal{P}_{mn}^{(p)}$ to the initial port configuration is equivalent to a weighted sum of these transformed port configurations according to (2). The weighting coefficients are the elements of the representation matrices (Table II). All computations presented in this section can be performed both graphically (Fig. 4–6) and analytically (appendix A).

The first antenna port is intended to act as a basis function of the first irreducible representation $\Gamma^{(1)}$ ($d_1 = 1$). Hence, the projection operator $\mathcal{P}_{11}^{(1)}$ with $p = 1$ is applied to the initial port configuration. In this case, however, the projection yields zero. This result simply means that a port configuration belonging to the first irreducible representation cannot be constructed with this setup. If a projection yields zero, another initial port configuration has to be chosen (see below).

The second antenna port is intended to act as a basis function of the second irreducible representation $\Gamma^{(2)}$ ($d_2 = 1$). Hence, the projection operator $\mathcal{P}_{11}^{(2)}$ with $p = 2$ is applied next. In this case, the projection yields a suitable port configuration as illustrated in Fig. 5(b).

The third irreducible representation $\Gamma^{(3)}$ is two-dimensional ($d_3 = 2$). Hence, two orthogonal basis functions belong to it. The third and the fourth antenna ports are intended to act as basis functions of this irreducible representation. According to (3), the index m (row index) distinguishes the two basis functions. Hence, either the projection operator $\mathcal{P}_{11}^{(3)}$ or $\mathcal{P}_{12}^{(3)}$ with $p = 3$ and $m = 1$ can be applied to construct the third port. Likewise, either $\mathcal{P}_{21}^{(3)}$ or $\mathcal{P}_{22}^{(3)}$ with $p = 3$ and $m = 2$ can be applied to construct the fourth port. The resulting port configurations are depicted in Fig. 5(c) and (d).

For the construction of the first port, it has been found that a delta-gap voltage source on a symmetry axis is not suitable. Therefore, the voltage source is now shifted to a half-edge

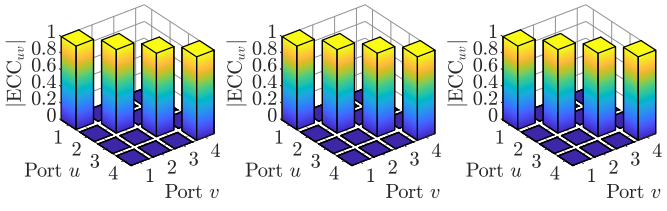

Fig. 7. Envelope correlation coefficients (ECC) of equilateral triangular plate with ports as defined in Fig. 6(b) and Fig. 5(b)–(d) for different circumradii R as functions of the wavelength λ. (a) $R = 0.5\lambda$. (b) $R = \lambda$. (c) $R = 2\lambda$.

center between two symmetry axes as illustrated in Fig. 6(a). The alternative impressed electric field strength $\mathbf{E}_{\mathrm{i},2}(\mathbf{r})$ is

$$\mathbf{E}_{\mathrm{i},2}(x,y) = V\delta\big(x - \frac{5}{4}r, y - \frac{\sqrt{3}}{4}r\big)\begin{pmatrix}\sqrt{3}/2\\ -1/2\end{pmatrix}. \qquad (5)$$

The application of $\mathcal{P}_{11}^{(1)}$ now yields a suitable port configuration as shown in Fig. 6(b).

In this work, antenna ports consisting of as few feed points as possible are considered optimal. As a general guideline, a single delta-gap voltage source placed on a symmetry axis should be used as the initial port configuration. Those ports which cannot be generated this way are subsequently constructed from the alternative initial port configuration consisting of a single delta-gap voltage source placed halfway between two symmetry axes. The applicability of this guideline will be confirmed by the examples in section III.

The orthogonality of the four antenna ports is now checked by means of the envelope correlation coefficients (ECC) [9]. To this end, the far field radiation patterns excited by the antenna ports are computed with the method of moments [30]. The ECC calculated from these radiation patterns are shown in Fig. 7, confirming the orthogonality of the four antenna ports.

III. Application Example

The literature review in section I reveals that multimode antennas with up to four uncorrelated antenna ports have been reported. By means of the methodology presented in this paper, in theory, an arbitrary number of orthogonal antenna ports can be constructed by choosing a suitable antenna geometry [9]. However, the practical implementation effort to be expected should be taken into account right from the beginning of the design process. This can now be done conveniently thanks to the a priori knowledge from the port construction procedure.

In order to demonstrate this, it is supposed that a multimode antenna with six orthogonal antenna ports is to be realized. A lot of different symmetric antenna geometries are suitable for this task from a theoretical point of view [9]. The best choice can thus only be made from a practical point of view. In particular, the feed network, which is required for connecting the antenna ports to the respective feed points, is expected to be a major source of complexity (cf. [14]–[17]).

In this example, a square plate and a regular hexagonal plate are analyzed as suitable basic antenna geometries. Planar geometries are chosen as they enable low-profile designs and integration capabilities (cf. [15], [17], and section IV).

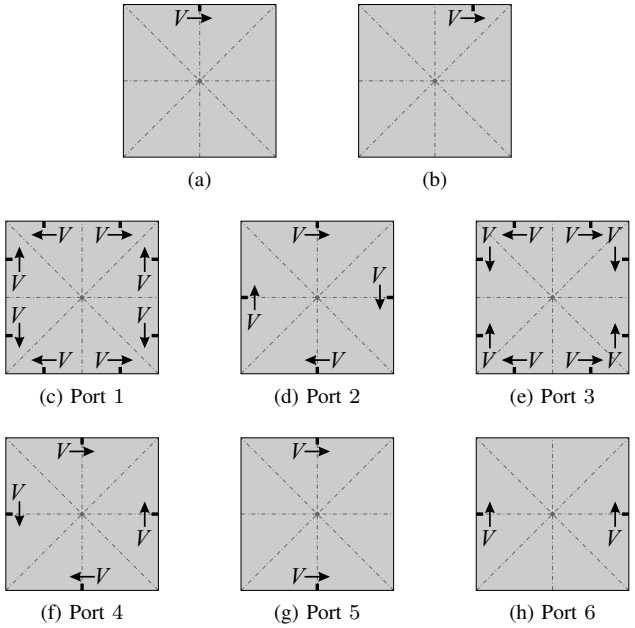

Fig. 8. Construction of orthogonal antenna ports on square plate. (a) Initial port configuration consisting of one delta-gap voltage source at edge center for constructing ports 2, 4, 5, and 6. (b) Alternative initial port configuration consisting of one delta-gap voltage source at half-edge center for constructing ports 1 and 3. (c)–(h) Constructed orthogonal antenna ports. Delta-gap voltage sources denoted by black lines and arrows.

A. Square Plate

The square plate is the regular polygonal plate of lowest order offering six orthogonal antenna ports [9]. The port construction procedure (section II-C) is now applied.

A single delta-gap voltage source placed at an edge center is taken as the initial port configuration, as depicted in Fig. 8(a). Applying the projection operators of the different irreducible representations to this initial port configuration yields the ports 2, 4, 5, and 6 as shown in Fig. 8(d), (f), (g), and (h), respectively. Four out of the six possible port configurations can be constructed this way. The two remaining ports 1 and 3 require an alternative initial port configuration on a half-edge center, as depicted in Fig. 8(b). Applying the projection operators of the remaining irreducible representations yields the port configurations shown in Fig. 8(c) and (e), respectively.

Again, two simple initial port configurations consisting each of one single delta-gap voltage source are sufficient for obtaining all optimal port configurations. The ports which are constructed from the same initial port configuration share the same feed points (ports 1 and 3 as well as ports 2, 4, 5, and 6). Consequently, two independent feed networks can be employed in order to drive the two sets of ports. Additionally, the feed points of all six ports are driven with the same source voltage (equal amplitude distribution). This has the consequence that the respective feed networks only have to adjust the phase relations between the feed points.

B. Regular Hexagonal Plate

The regular hexagonal plate offers a maximum of eight orthogonal antenna ports [9]. Of course, there is nothing to be said against realizing only six ports.

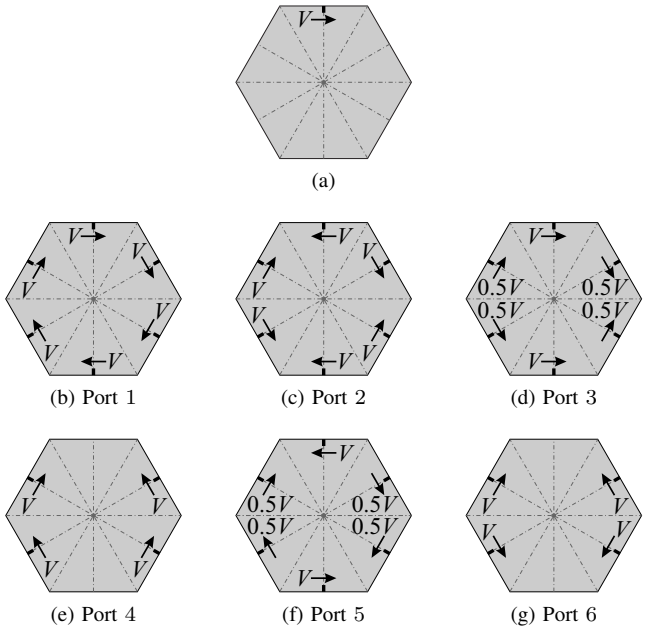

Fig. 9. Construction of orthogonal antenna ports on regular hexagonal plate. (a) Initial port configuration consisting of one delta-gap voltage source at edge center for constructing ports 1 to 6. (b)–(g) Constructed orthogonal antenna ports. Delta-gap voltage sources denoted by black lines and arrows.

Once again, the initial port configuration consists of a single delta-gap voltage source at an edge center (Fig. 9(a)). In the case of the hexagonal plate, this initial port configuration is already sufficient in order to generate six optimal port configurations (Fig. 9(b)–(g)).

In contrast to the square plate, all six ports share the same feed points. Consequently, a single feed network is necessary in order to drive all six ports. At first glance, a single feed network may appear as an advantage compared to the square plate. However, the more ports per feed network, the more decoupling effort has to be spent, necessitating more components and thus a bulkier network. In addition, the ports 3 and 5 demand an unequal amplitude distribution.

It is thus estimated that the square plate requires less implementation effort. Although two feed networks are necessary, these only have to handle two and four antenna ports, respectively, with equal amplitude distribution. As will become apparent in section IV, a low feed network complexity is important for a reasonable antenna performance.

This example demonstrates how the a priori knowledge about the optimal port configurations can be exploited in order to identify a suitable geometry for a multimode antenna design with a desired number of orthogonal ports. As a general guideline, a higher number of ports requires a higher symmetry order. A higher symmetry order, however, requires more feed points per port and thus more complicated feed networks. The number of ports is thus primarily a question of how much implementation effort is to be spent.

IV. Prototype

In order to demonstrate that the port construction procedure can be used to design a multimode antenna with uncorrelated

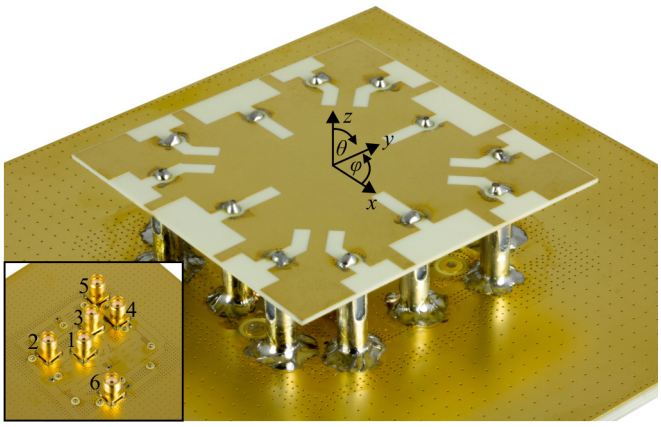

Fig. 10. Photograph of the fabricated six-port multimode antenna showing the antenna element, the coaxial baluns, and layer 1 (top layer) of the feed network (ground plane). The depicted coordinate system serves as reference for the radiation patterns. The inset shows layer 5 (bottom layer) of the feed network with the six antenna ports realized as surface-mount SMA connectors.

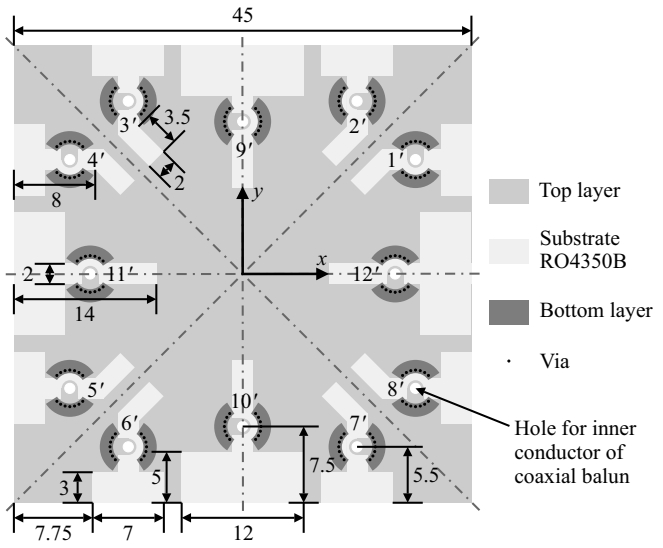

Fig. 11. Layout of the final antenna element. The actual antenna surface with square symmetry is placed on the top layer. Stepped excitation slots replace the ideal delta-gap voltage sources. The feed points for connecting the coaxial baluns are denoted by the primed numbers. The solder pads on the bottom layer connect the slotted outer conductors of the coaxial baluns to the top layer by means of through-hole vias. Dimensions in mm.

antenna ports from scratch, a prototype is fabricated. As discussed in section III, a square geometry is a reasonable choice enabling six ports with the least implementation effort. Hence, the optimal port configurations in Fig. 8(c)–(h) are used as the starting point of the design process.

The principal design step consists of introducing practical excitation elements in order to enable impedance matching. Furthermore, a feed network is required in order to distribute the port signals to the respective feed points with the correct phase relations. Inspired by the four-port designs in [15] and [17], the planar antenna element is positioned at a certain height above a ground plane. The feed network is integrated below this ground plane. The two parts are joined together by baluns. In order to give an impression of the design concept, a photograph of the fabricated prototype is shown in Fig. 10. The multimode antenna is intended to operate within the ultra-wide frequency band from $6\,\mathrm{GHz}$ to $8.5\,\mathrm{GHz}$ [32], [33].

A. Antenna Element

The layout of the final antenna element is depicted in Fig. 11. The square plate is mounted on the top layer of a Rogers RO4350B substrate with the height $508\,\mu\mathrm{m}$. Based on a characteristic mode analysis, the edge length is chosen to be $45\,\mathrm{mm}$. This is the minimum size so that for each antenna port at least one characteristic mode is significant [31].

The ideal delta-gap voltage sources of the constructed optimal port configurations can be readily replaced by practical excitation slots [15], [31]. The slot positions along the plate edges (edge centers, half-edge centers) are directly adopted from the port configurations in Fig. 8(c)–(h). The feed points within the excitation slots are denoted by the primed numbers in Fig. 11. At these points, the feed network has to provide the correct relative phases as required by the optimal port configurations (denoted by the voltage directions in Fig. 8).

As detailed in [31], the input impedances of the six antenna ports can be controlled flexibly by adjusting the slot lengths, the slot widths, and the feed point positions within the slots. These parameters are optimized systematically in such a way that the antenna ports are matched sufficiently to $50\,\Omega$, yielding the dimensions shown in Fig. 11. The use of stepped excitation slots provides a broader bandwidth [17], [31]. In this context, the minimum height above the ground plane is found to be $12.5\,\mathrm{mm}$. While optimizing the antenna element, the square symmetry must be preserved in order to ensure the orthogonality of the antenna ports. Although the original characteristic modes are perturbed by the excitation slots, the symmetry guarantees that the ports still excite mutually exclusive sets of modes [9].

In order to connect the feed points within the excitation slots to the feed network below the ground plane, semi-rigid coaxial cables are employed [15]. As the excitation slots act as symmetric terminations, the outer conductors are slotted in order to serve as baluns [34]. The inner conductor of the coaxial balun is passed through the substrate and connected to one side of the excitation slot (see Fig. 11). The slotted outer conductor is connected to both sides of the excitation slot by means of through-hole vias from the bottom layer.

B. Feed Network

There are two sets of feed points. The complete feed network thus consists of two sub-networks: One for the ports 1 and 3, and one for the ports 2, 4, 5, and 6. Hence, it suggests itself to realize the feed network in multilayer technology.

The layout of the feed network is shown in Fig. 12. The feed point positions denoted by the primed numbers are dictated by the antenna element (Fig. 11). Additionally, the size of the feed network is restricted to an area of $45\,\mathrm{mm} \times 45\,\mathrm{mm}$ so that it fits entirely below the antenna element.

The chosen layer setup consists of five metal layers. Layer 1 (top layer) serves as the ground plane for the antenna element (not shown in Fig. 12, see Fig. 10). The feed

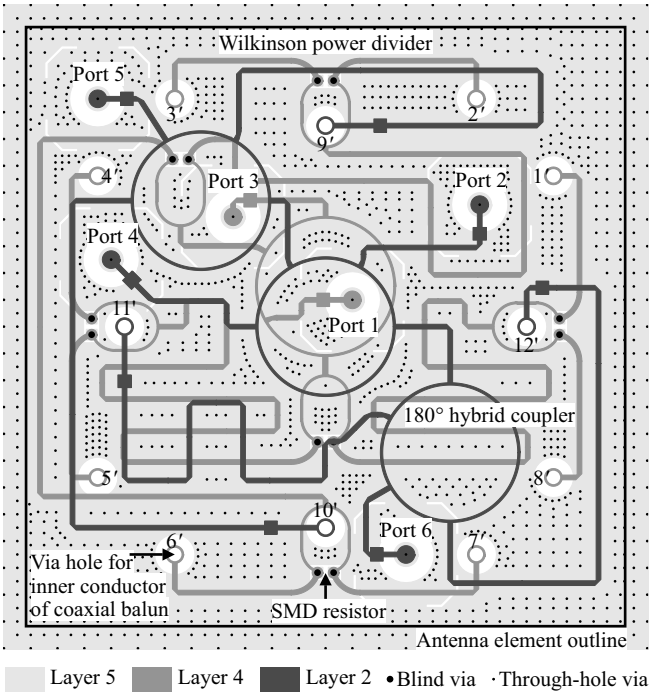

Fig. 12. Layout of the feed network. The network layers 2 and 4 as well as the ground layer 5 and all vias are displayed.

network for the ports 2, 4, 5, and 6 is realized in stripline technology [35] on layer 2. The feed network for the ports 1 and 3 is realized in stripline technology on layer 4. The two network layers are separated by the ground layer 3 (not shown in Fig. 12). Layer 5 (bottom layer) serves as the lower ground plane. Additionally, the resistors required for the Wilkinson power dividers are placed on this layer and connected to layer 4 by means of blind vias. The three ground layers 1, 3, and 5 are linked by means of through-hole vias.

180° hybrid couplers and Wilkinson power dividers [35] are employed in order to distribute the port signals to the respective feed points with the required phase relations and decouple those ports which share the same feed points (Fig. 12). The 180° hybrid couplers are realized as ring couplers (rat-race couplers). 100 Ω-SMD resistors of size 0402, which are mounted on layer 5, are used for the Wilkinson power dividers. The stripline lengths are adjusted in such a way that no additional phase differences are added.

The antenna ports themselves are realized as surface-mount SMA connectors placed on layer 5 (Fig. 10). They are connected to the respective network layers by means of through-hole vias. The outer conductors of the coaxial baluns are soldered to the ground plane on layer 1 (Fig. 10). The inner conductors are connected to the respective network layer by means of through-hole vias. All coaxial-to-stripline transitions are designed to minimize signal reflections. For the measurements and the final simulations, a finite square ground plane of dimensions $90\,\mathrm{mm} \times 90\,\mathrm{mm}$ is realized (Fig. 10).

C. Simulation and Measurement Results

The measured and simulated S-parameters of the six-port multimode antenna are shown in Fig. 13. The antenna ports

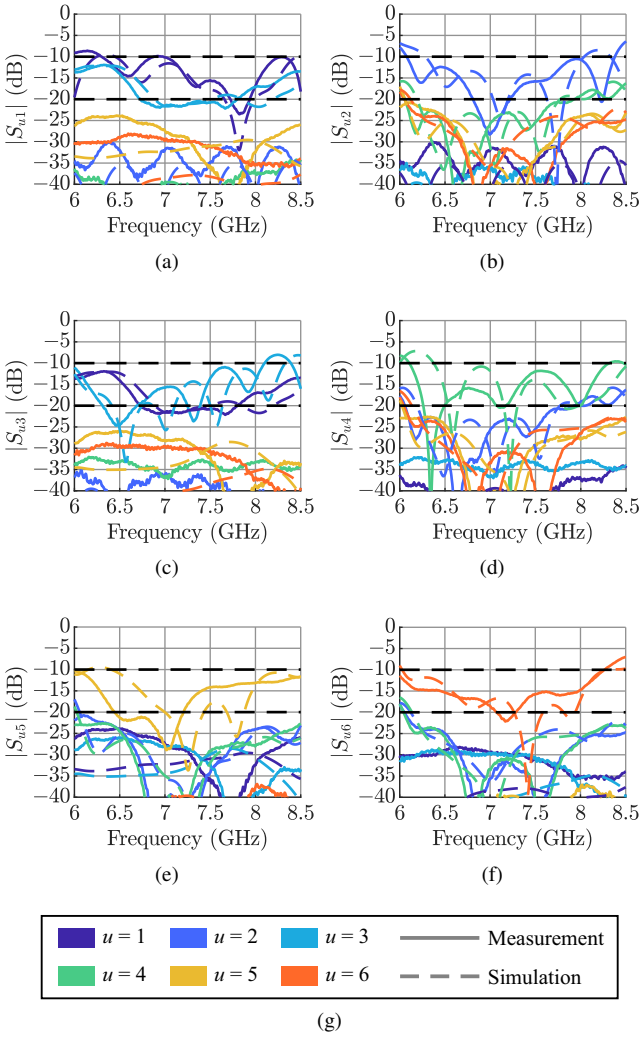

Fig. 13. Measured and simulated S-parameters S_{uv} (absolute values) from the v-th port to the u-th port of the fabricated multimode antenna. (a) Port 1 active ($v = 1$). (b) Port 2 active ($v = 2$). (c) Port 3 active ($v = 3$). (d) Port 4 active ($v = 4$). (e) Port 5 active ($v = 5$). (f) Port 6 active ($v = 6$). (g) Legend.

are sufficiently matched to 50 Ω ($|S_{uu}| \leq -10\,\mathrm{dB}$) and sufficiently decoupled ($|S_{uv}| \leq -20\,\mathrm{dB}$) over almost the entire frequency range of interest. Deviations occur towards the limits of the frequency range which can be attributed to the fact that the feed network consists of narrowband components.

The measured and simulated realized gains of the far field radiation patterns excited by the six antenna ports at the center frequency are shown in Fig. 14. It is evident that the fabricated prototype reproduces the radiation patterns predicted by the simulation model very well. A more detailed analysis of the radiation patterns is not conducted here as the port correlation is of more importance.

The inspection of the ECC in Fig. 15 computed from the far field radiation patterns confirms that the antenna ports are only weakly correlated. The maximum correlation coefficient is approximately 0.05. From a practical point of view, the antenna ports can thus be termed uncorrelated. Turning back to Fig. 14, it is deduced that the antenna ports offer a combination of pattern and polarization diversity, as intended.

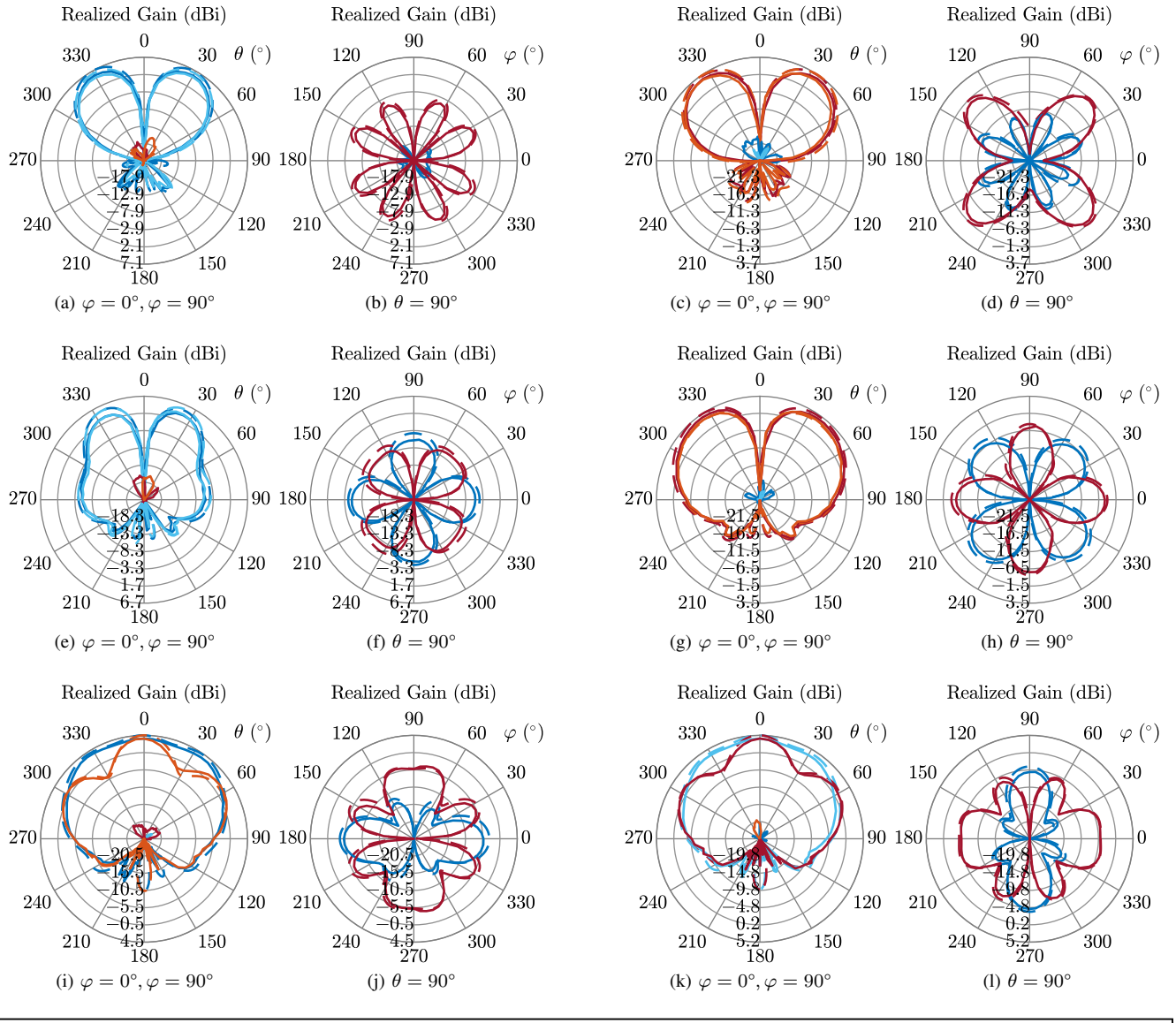

Fig. 14. Measured and simulated realized gains of the fabricated six-port multimode antenna at 7.25 GHz in xz-plane ($\varphi = 0°$), yz-plane ($\varphi = 90°$), and xy-plane ($\theta = 90°$) with respect to the coordinate system in Fig. 10. All plots are limited to the maximum realized gain of the respective port and display a dynamic range of 30 dB. (a)–(b) Port 1. (c)–(d) Port 2. (e)–(f) Port 3. (g)–(h) Port 4. (i)–(j) Port 5. (k)–(l) Port 6. (m) Legend.

The total efficiencies [34] of the fabricated multimode antenna computed from the measured realized gains are listed in Table III. The feed network is identified as the principal cause for dielectric and conduction losses.

TABLE III
TOTAL EFFICIENCIES OF THE FABRICATED SIX-PORT MULTIMODE ANTENNA COMPUTED FROM MEASURED REALIZED GAINS AT 7.25 GHz.

Antenna port	1	2	3	4	5	6
Total efficiency (%)	62.3	50.5	63.3	44.0	51.1	52.8

V. CONCLUSION

A systematic port construction procedure for arbitrary symmetric multimode antennas is presented. It is based on the projection operators from group theory. The optimal orthogonal port configurations are thus solely determined by the symmetry of an antenna. In particular, they are independent of the electrical size and hence independent of frequency.

In addition, the proposed procedure is a completely analytical method. No electromagnetic simulations or modal analyses are required. Although fundamentally rooted in the theory of symmetry, it has direct practical consequences for a successful multimode antenna design. As the optimal port configurations are known a priori, different suitable antenna geometries can be compared with respect to their port potential and the estimated implementation effort.

In this regard, the feed network is identified as the principal

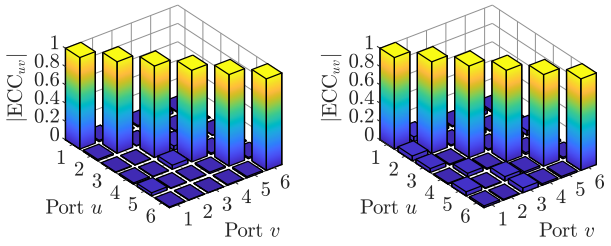

Fig. 15. Envelope correlation coefficients (ECC) of the fabricated six-port multimode antenna at 7.25 GHz. (a) Computed from simulated radiation patterns. (b) Computed from measured radiation patterns.

source of complexity for multimode antenna design. Although antenna geometries with a higher symmetry order offer more orthogonal antenna ports, the complexity of the feed network grows as well. This assessment is corroborated by the fabricated prototype, where the feed network adds complexity due to a potentially challenging layout and the introduction of bandwidth limitations, coupling, and losses. Nevertheless, this complexity can now be estimated a priori thanks to the knowledge about the optimal port configurations.

The practical applicability of the proposed design method is confirmed by the fabricated prototype. Starting with the optimal port configurations derived analytically from the symmetry of a square plate, a complete six-port multimode antenna is realized whose ports are sufficiently matched, decoupled, and decorrelated over a reasonable bandwidth.

Appendix A
Analytical Computations

This appendix provides details about the computations conducted throughout this paper. It is emphasized that all computations can be performed analytically.

In order to employ the transformation operators $P(T)$ according to (1), which are required for the projection operators, the orthogonal rotation matrices $\mathbf{R}(T)$ are needed:

$$\mathbf{R}(T) = \begin{pmatrix} R_{11}(T) & R_{12}(T) \\ R_{21}(T) & R_{22}(T) \end{pmatrix}, \quad \mathbf{R}^{-1}(T) = \mathbf{R}^{\mathrm{T}}(T). \tag{6}$$

For a rotation by Φ about an arbitrary axis through the coordinate origin whose direction is denoted by the unit vector $\mathbf{n} = (n_x, n_y, n_z)^{\mathrm{T}}$, the elements of (6) are [28]:

$$R_{11}(\Phi) = n_x^2(1-\cos\Phi) + \cos\Phi, \tag{7a}$$
$$R_{12}(\Phi) = n_x n_y(1-\cos\Phi) + n_z \sin\Phi, \tag{7b}$$
$$R_{21}(\Phi) = n_y n_x(1-\cos\Phi) - n_z \sin\Phi, \tag{7c}$$
$$R_{22}(\Phi) = n_y^2(1-\cos\Phi) + \cos\Phi. \tag{7d}$$

As an example, the rotation matrices of the symmetry group of the equilateral triangular plate are listed in Table IV.

These are now used to compute the transformation of the impressed electric field strength $\mathbf{E}_{\mathrm{i}}(\mathbf{r})$ of the initial port configuration given in (4) by means of (1):

$$P(T)\mathbf{E}_{\mathrm{i}}(x,y) = \mathbf{R}(T)\mathbf{E}_{\mathrm{i}}\big(\mathbf{R}^{\mathrm{T}}(T)\mathbf{r}\big) \tag{8}$$
$$= \begin{pmatrix} R_{11}(T) & R_{12}(T) \\ R_{21}(T) & R_{22}(T) \end{pmatrix} \mathbf{E}_{\mathrm{i}}\Big(\begin{pmatrix} R_{11}(T) & R_{21}(T) \\ R_{12}(T) & R_{22}(T) \end{pmatrix} \begin{pmatrix} x \\ y \end{pmatrix}\Big).$$

This equation states that in (4) the x-coordinate is replaced by $R_{11}(T)x + R_{21}(T)y$ and the y-coordinate is replaced by $R_{12}(T)x + R_{22}(T)y$ and the resulting vector-valued function is left-multiplied by $\mathbf{R}(T)$. The results for the six symmetry operations of the equilateral triangular plate are given in (9), which correspond to the transformed delta-gap voltage sources as depicted in Fig. 4.

These results can now be applied directly to the computation of the optimal port configurations:

$$\mathcal{P}_{11}^{(1)}\mathbf{E}_{\mathrm{i}}(x,y) = \frac{1}{6}\Big(P(E) + P(C_{3z}) + P(C_{3z}^2) + P(C_{2x}) + P(C_{2A}) + P(C_{2B})\Big)\mathbf{E}_{\mathrm{i}}(x,y), \tag{10a}$$
$$\mathcal{P}_{11}^{(2)}\mathbf{E}_{\mathrm{i}}(x,y) = \frac{1}{6}\Big(P(E) + P(C_{3z}) + P(C_{3z}^2) - P(C_{2x}) - P(C_{2A}) - P(C_{2B})\Big)\mathbf{E}_{\mathrm{i}}(x,y), \tag{10b}$$
$$\mathcal{P}_{11}^{(3)}\mathbf{E}_{\mathrm{i}}(x,y) = \frac{1}{3}\Big(P(E) - \frac{1}{2}P(C_{3z}) - \frac{1}{2}P(C_{3z}^2) + P(C_{2x}) - \frac{1}{2}P(C_{2A}) - \frac{1}{2}P(C_{2B})\Big)\mathbf{E}_{\mathrm{i}}(x,y), \tag{10c}$$
$$\mathcal{P}_{12}^{(3)}\mathbf{E}_{\mathrm{i}}(x,y) = \frac{1}{3}\Big(\frac{\sqrt{3}}{2}P(C_{3z}) - \frac{\sqrt{3}}{2}P(C_{3z}^2) + \frac{\sqrt{3}}{2}P(C_{2A}) - \frac{\sqrt{3}}{2}P(C_{2B})\Big)\mathbf{E}_{\mathrm{i}}(x,y), \tag{10d}$$
$$\mathcal{P}_{21}^{(3)}\mathbf{E}_{\mathrm{i}}(x,y) = \frac{1}{3}\Big(-\frac{\sqrt{3}}{2}P(C_{3z}) + \frac{\sqrt{3}}{2}P(C_{3z}^2) + \frac{\sqrt{3}}{2}P(C_{2A}) - \frac{\sqrt{3}}{2}P(C_{2B})\Big)\mathbf{E}_{\mathrm{i}}(x,y), \tag{10e}$$
$$\mathcal{P}_{22}^{(3)}\mathbf{E}_{\mathrm{i}}(x,y) = \frac{1}{3}\Big(P(E) - \frac{1}{2}P(C_{3z}) - \frac{1}{2}P(C_{3z}^2) - P(C_{2x}) + \frac{1}{2}P(C_{2A}) + \frac{1}{2}P(C_{2B})\Big)\mathbf{E}_{\mathrm{i}}(x,y). \tag{10f}$$

The optimal port configurations are simply weighted sums of the transformed delta-gap voltage sources. The computations with $\mathbf{E}_{\mathrm{i},2}$ (5) can be performed in the same way (cf. Fig. 6).

The analytical computations described in this appendix are applicable to arbitrary point groups and were also used to derive the results presented in section III.

References

[1] L. C. Godara, "Applications of antenna arrays to mobile communications. I. Performance improvement, feasibility, and system considerations," *Proceedings of the IEEE*, vol. 85, no. 7, pp. 1031–1060, 1997.

[2] J. Mietzner, R. Schober, L. Lampe, W. H. Gerstacker, and P. A. Hoeher, "Multiple-antenna techniques for wireless communications – a comprehensive literature survey," *IEEE Communications Surveys Tutorials*, vol. 11, no. 2, pp. 87–105, 2009.

[3] C. Waldschmidt and W. Wiesbeck, "Compact wide-band multimode antennas for MIMO and diversity," *IEEE Transactions on Antennas and Propagation*, vol. 52, no. 8, pp. 1963–1969, 2004.

TABLE IV
ROTATION MATRICES OF THE SYMMETRY GROUP OF THE EQUILATERAL TRIANGULAR PLATE.

T	E	C_{3z}	C_{3z}^2	C_{2x}	C_{2A}	C_{2B}
$\mathbf{R}(T)$	$\begin{pmatrix} 1 & 0 \\ 0 & 1 \end{pmatrix}$	$\begin{pmatrix} -\frac{1}{2} & \frac{\sqrt{3}}{2} \\ -\frac{\sqrt{3}}{2} & -\frac{1}{2} \end{pmatrix}$	$\begin{pmatrix} -\frac{1}{2} & -\frac{\sqrt{3}}{2} \\ \frac{\sqrt{3}}{2} & -\frac{1}{2} \end{pmatrix}$	$\begin{pmatrix} 1 & 0 \\ 0 & -1 \end{pmatrix}$	$\begin{pmatrix} -\frac{1}{2} & \frac{\sqrt{3}}{2} \\ \frac{\sqrt{3}}{2} & \frac{1}{2} \end{pmatrix}$	$\begin{pmatrix} -\frac{1}{2} & -\frac{\sqrt{3}}{2} \\ -\frac{\sqrt{3}}{2} & \frac{1}{2} \end{pmatrix}$

$$P(E)\mathbf{E}_\mathrm{i}(x,y) = V\delta\big(x-\frac{1}{2}r, y-\frac{\sqrt{3}}{2}r\big)\begin{pmatrix}\sqrt{3}/2\\-1/2\end{pmatrix} \tag{9a}$$

$$P(C_{3z})\mathbf{E}_\mathrm{i}(x,y) = V\delta\big(-\frac{1}{2}x-\frac{\sqrt{3}}{2}y-\frac{1}{2}r, \frac{\sqrt{3}}{2}x-\frac{1}{2}y-\frac{\sqrt{3}}{2}r\big)\begin{pmatrix}-\sqrt{3}/4-\sqrt{3}/4\\-3/4+1/4\end{pmatrix} = V\delta\big(x-\frac{1}{2}r, y+\frac{\sqrt{3}}{2}r\big)\begin{pmatrix}-\sqrt{3}/2\\-1/2\end{pmatrix} \tag{9b}$$

$$P(C_{3z}^2)\mathbf{E}_\mathrm{i}(x,y) = V\delta\big(-\frac{1}{2}x+\frac{\sqrt{3}}{2}y-\frac{1}{2}r, -\frac{\sqrt{3}}{2}x-\frac{1}{2}y-\frac{\sqrt{3}}{2}r\big)\begin{pmatrix}-\sqrt{3}/4+\sqrt{3}/4\\3/4+1/4\end{pmatrix} = V\delta\big(x+r, y\big)\begin{pmatrix}0\\1\end{pmatrix} \tag{9c}$$

$$P(C_{2x})\mathbf{E}_\mathrm{i}(x,y) = V\delta\big(x-\frac{1}{2}r, -y-\frac{\sqrt{3}}{2}r\big)\begin{pmatrix}\sqrt{3}/2\\1/2\end{pmatrix} = V\delta\big(x-\frac{1}{2}r, y+\frac{\sqrt{3}}{2}r\big)\begin{pmatrix}\sqrt{3}/2\\1/2\end{pmatrix} \tag{9d}$$

$$P(C_{2A})\mathbf{E}_\mathrm{i}(x,y) = V\delta\big(-\frac{1}{2}x+\frac{\sqrt{3}}{2}y-\frac{1}{2}r, \frac{\sqrt{3}}{2}x+\frac{1}{2}y-\frac{\sqrt{3}}{2}r\big)\begin{pmatrix}-\sqrt{3}/4-\sqrt{3}/4\\3/4-1/4\end{pmatrix} = V\delta\big(x-\frac{1}{2}r, y-\frac{\sqrt{3}}{2}r\big)\begin{pmatrix}-\sqrt{3}/2\\1/2\end{pmatrix} \tag{9e}$$

$$P(C_{2B})\mathbf{E}_\mathrm{i}(x,y) = V\delta\big(-\frac{1}{2}x-\frac{\sqrt{3}}{2}y-\frac{1}{2}r, -\frac{\sqrt{3}}{2}x+\frac{1}{2}y-\frac{\sqrt{3}}{2}r\big)\begin{pmatrix}-\sqrt{3}/4+\sqrt{3}/4\\-3/4-1/4\end{pmatrix} = V\delta\big(x+r, y\big)\begin{pmatrix}0\\-1\end{pmatrix} \tag{9f}$$

[4] C.-N. Chuah, D. N. C. Tse, J. M. Kahn, and R. A. Valenzuela, "Capacity scaling in MIMO wireless systems under correlated fading," *IEEE Transactions on Information Theory*, vol. 48, no. 3, pp. 637–650, 2002.

[5] D. Manteuffel, "MIMO antenna design challenges," in *2009 Loughborough Antennas & Propagation Conference*, Nov 2009, pp. 50–56.

[6] R. Garbacz and R. Turpin, "A generalized expansion for radiated and scattered fields," *IEEE Transactions on Antennas and Propagation*, vol. 19, no. 3, pp. 348–358, May 1971.

[7] R. Harrington and J. Mautz, "Theory of characteristic modes for conducting bodies," *IEEE Transactions on Antennas and Propagation*, vol. 19, no. 5, pp. 622–628, Sep 1971.

[8] Y. Chen and C. Wang, *Characteristic Modes: Theory and Applications in Antenna Engineering*. Hoboken, NJ, USA: John Wiley & Sons, 2015.

[9] N. Peitzmeier and D. Manteuffel, "Upper bounds and design guidelines for realizing uncorrelated ports on multimode antennas based on symmetry analysis of characteristic modes," *IEEE Transactions on Antennas and Propagation*, vol. 67, no. 6, pp. 3902–3914, 2019.

[10] S. K. Chaudhury, W. L. Schroeder, and H. J. Chaloupka, "MIMO antenna system based on orthogonality of the characteristic modes of a mobile device," in *2007 2nd International ITG Conference on Antennas*, March 2007, pp. 58–62.

[11] E. Antonino-Daviu, M. Cabedo-Fabres, M. Gallo, M. Ferrando-Bataller, and M. Bozzetti, "Design of a multimode MIMO antenna using characteristic modes," in *2009 3rd European Conference on Antennas and Propagation*, 2009, pp. 1840–1844.

[12] S. K. Chaudhury, H. J. Chaloupka, and A. Ziroff, "Multiport antenna systems for MIMO and diversity," in *Proceedings of the Fourth European Conference on Antennas and Propagation*, April 2010, pp. 1–5.

[13] R. Martens, E. Safin, and D. Manteuffel, "Selective excitation of characteristic modes on small terminals," in *Proceedings of the 5th European Conference on Antennas and Propagation (EuCAP)*, April 2011, pp. 2492–2496.

[14] R. Martens and D. Manteuffel, "Systematic design method of a mobile multiple antenna system using the theory of characteristic modes," *IET Microwaves, Antennas & Propagation*, vol. 8, no. 12, pp. 887–893, Sep. 2014.

[15] D. Manteuffel and R. Martens, "Compact multimode multielement antenna for indoor UWB massive MIMO," *IEEE Transactions on Antennas and Propagation*, vol. 64, no. 7, pp. 2689–2697, 2016.

[16] M. Bouezzeddine and W. L. Schroeder, "Design of a wideband, tunable four-port MIMO antenna system with high isolation based on the theory of characteristic modes," *IEEE Transactions on Antennas and Propagation*, vol. 64, no. 7, pp. 2679–2688, July 2016.

[17] W. Su, Q. Zhang, S. Alkaraki, Y. Zhang, X. Zhang, and Y. Gao, "Radiation energy and mutual coupling evaluation for multimode MIMO antenna based on the theory of characteristic mode," *IEEE Transactions on Antennas and Propagation*, vol. 67, no. 1, pp. 74–84, 2019.

[18] N. Peitzmeier and D. Manteuffel, "Systematic design method for asymmetric multiport antennas based on characteristic modes," in *2020 14th European Conference on Antennas and Propagation (EuCAP)*, 2020, pp. 1–5.

[19] ——, "Selective excitation of characteristic modes on an electrically large antenna for MIMO applications," in *12th European Conference on Antennas and Propagation (EuCAP 2018)*, April 2018, pp. 1–5.

[20] K. R. Schab, J. M. Outwater, and J. T. Bernhard, "Classifying characteristic mode crossing avoidances with symmetry and energy coupling," in *2016 IEEE International Symposium on Antennas and Propagation (APSURSI)*, June 2016, pp. 13–14.

[21] K. R. Schab and J. T. Bernhard, "A group theory rule for predicting eigenvalue crossings in characteristic mode analyses," *IEEE Antennas and Wireless Propagation Letters*, vol. 16, pp. 944–947, 2017.

[22] M. Masek, M. Capek, L. Jelinek, and K. Schab, "Utilization of symmetries in method of moments," in *2019 IEEE International Symposium on Antennas and Propagation and USNC-URSI Radio Science Meeting*, 2019, pp. 2191–2192.

[23] M. Masek, M. Capek, and L. Jelinek, "Feeding positions providing the lowest TARC of uncorrelated channels," in *2020 14th European Conference on Antennas and Propagation (EuCAP)*, 2020, pp. 1–5.

[24] M. Masek, M. Capek, L. Jelinek, and K. Schab, "Modal tracking based on group theory," *IEEE Transactions on Antennas and Propagation*, vol. 68, no. 2, pp. 927–937, Feb 2020.

[25] J. Knorr, "Consequences of symmetry in the computation of characteristic modes for conducting bodies," *IEEE Transactions on Antennas and Propagation*, vol. 21, no. 6, pp. 899–902, Nov 1973.

[26] L. D. Landau and E. M. Lifshitz, *Quantum Mechanics: Non-Relativistic Theory*, 3rd ed., ser. Course of Theoretical Physics. Oxford, UK: Pergamon Press, 1977, ch. XII. The Theory of Symmetry.

[27] G. F. Koster, *Properties of the Thirty-Two Point Groups*. Cambridge, MA, USA: M.I.T. Press, 1963.

[28] J. F. Cornwell, *Group Theory in Physics: An Introduction*. San Diego, CA, USA: Academic Press, 1997.

[29] M. Tinkham, *Group Theory and Quantum Mechanics*. New York, NY, USA: McGraw-Hill, 1964.

[30] S. N. Makarov, *Antenna and EM Modeling with MATLAB*. Hoboken, NJ, USA: John Wiley & Sons, 2002.

[31] N. Peitzmeier and D. Manteuffel, "Systematic design of an ultra-wideband six-port multi-mode antenna element using symmetry properties of characteristic modes," in *2019 International Conference on Electromagnetics in Advanced Applications (ICEAA)*, 2019, pp. 466–471.

[32] P. A. Hoeher, D. Manteuffel, N. Doose, and N. Peitzmeier, "Ultra-wideband massive MIMO communications using multi-mode antennas," *Frequenz*, vol. 71, no. 9-10, pp. 439–448, 2017.
[33] N. L. Johannsen, N. Peitzmeier, P. A. Hoeher, and D. Manteuffel, "On the feasibility of multi-mode antennas in UWB and IoT applications below 10 GHz," *IEEE Communications Magazine*, vol. 58, no. 3, pp. 69–75, 2020.
[34] C. A. Balanis, *Antenna Theory: Analysis and Design*, 3rd ed. Hoboken, NJ, USA: John Wiley & Sons, 2005.
[35] D. M. Pozar, *Microwave Engineering*, 2nd ed. New York, NY, USA: John Wiley & Sons, 1998.

Nikolai Peitzmeier (S'17-M'21) was born in Lübbecke, Germany, in 1988. He received the B.Sc. and M.Sc. degrees in electrical engineering and information technology from Leibniz University Hannover, Germany, in 2013 and 2014, respectively.

Since then, he has been a Research Assistant with the Institute of Microwave and Wireless Systems, Leibniz University Hannover. His current research is focused on antenna design for MIMO applications, including beamforming and massive MIMO, based on the theory of characteristic modes in conjunction with the theory of symmetry. Further fields of interest are electromagnetic theory and simulation techniques as well as electromagnetic compatibility.

Tim Hahn was born in Hannover, Germany, in 1997. He received the B.Sc. degree in electrical engineering and information technology from Leibniz University Hannover, Germany, in 2020, where he is currently pursuing his M.Sc. degree.

His primary research interest is focused on MIMO antenna design for base stations and mobile terminals utilizing the theory of characteristic modes as well as antenna integration for millimeter wave communication systems. Some of his further fields of interest include beamforming techniques for massive MIMO arrays, computational electromagnetics, and RF circuit design.

Dirk Manteuffel (M'09) was born in Issum, Germany, in 1970. He received the Dipl.-Ing. and Dr.-Ing. degrees in electrical engineering from the University of Duisburg-Essen, Essen, Germany, in 1998 and 2002, respectively.

From 1998 to 2009, he was with IMST, Kamp-Lintfort, Germany. As a Project Manager, he was responsible for industrial antenna development and advanced projects in the field of antennas and EM modeling. From 2009 to 2016, he was a Full Professor of wireless communications at Christian-Albrechts-University, Kiel, Germany. Since June 2016, he has been a Full Professor and the Director of the Institute of Microwave and Wireless Systems, Leibniz University Hannover, Hannover, Germany. His research interests include antenna integration and EM modeling for mobile communications and biomedical applications.

Dr. Manteuffel was the recipient of the Young Scientist Award of the Vodafone Foundation for Science in 2004 for his research on the analysis and design of integrated mobile phone antennas with special emphasis on the interaction with the user.